



Lab on a Chip

Enrichment of rare events using a multi-parameter high throughput microfluidic droplet sorter

Journal:	<i>Lab on a Chip</i>
Manuscript ID	LC-ART-08-2019-000790.R1
Article Type:	Paper
Date Submitted by the Author:	30-Dec-2019
Complete List of Authors:	Hung, Sheng-Ting; University of Colorado, JILA Mukherjee, Srijit; University of Colorado, JILA; University of Colorado, Department of Chemistry and Biochemistry Jimenez, Ralph; University of Colorado, JILA and Department of Chemistry and Biochemistry; National Institutes of Standards and Technology,

SCHOLARONE™
Manuscripts

1 Enrichment of rare events using a multi- 2 parameter high throughput microfluidic droplet 3 sorter

4
5 *Sheng-Ting Hung^a, Srijit Mukherjee^{a,b}, Ralph Jimenez^{a,b}*

6
7 ^aJILA, NIST and University of Colorado, Boulder, Colorado 80309, United States

8 ^bDepartment of Chemistry, University of Colorado, Boulder, Colorado 80309, United States

9

10 Abstract

11

12 High information content analysis, enrichment, and selection of rare events from a large population
13 are of great importance in biological and biomedical research. The fluorescence lifetime of a
14 fluorophore, a photophysical property which is independent of and complementary to fluorescence
15 intensity, has been incorporated into various imaging and sensing techniques through microscopy,
16 flow cytometry and droplet microfluidics. However, the throughput of fluorescence lifetime
17 activated droplet sorting is orders of magnitude lower than that of fluorescence activated cell
18 sorting, making it unattractive for applications such as directed evolution of enzymes, despite its
19 highly effective compartmentalization of library members. We developed a microfluidic sorter
20 capable of selecting fluorophores based on fluorescence lifetime and brightness at two excitation
21 and emission colors at a maximum droplet rate of 2.5 kHz. We also present a novel selection
22 strategy for efficiently analyzing and/or enriching rare fluorescent members from a large
23 population which capitalizes on the Poisson distribution of analyte encapsulation into droplets.
24 The effectiveness of the droplet sorter and the new selection strategy are demonstrated by enriching
25 rare populations from a $\sim 10^8$ -member site-directed mutagenesis library of fluorescent proteins
26 expressed in bacteria. This selection strategy can in principle be employed on many droplet sorting
27 platforms, and thus can potentially impact broad areas of science where analysis and enrichment
28 of rare events is needed.

29

30 Introduction

31

32 Fluorescence lifetime is an intrinsic molecular property that is independent of excitation and
33 emission intensity, local fluorophore concentration, and can be detected even with spectral
34 overlaps among fluorophores and in the presence of cellular auto-fluorescence. Fluorophore
35 lifetime is often sensitive to the solvent and biochemical environment, so it has been used as a
36 detection parameter in imaging and sensing techniques¹⁻⁴. In particular, fluorescence lifetime
37 imaging microscopy (FLIM) is a powerful tool complementing fluorescence brightness-based
38 imaging methods. It has been applied to subcellular pH measurements^{5,6}, intracellular refractive
39 index sensing^{7,8}, molecular interactions in cells⁹⁻¹¹, drug evaluation and discovery¹²⁻¹⁴, drug
40 delivery and cancer studies¹⁵⁻¹⁸. Nonetheless, FLIM applications are hampered by its throughput.
41 Flow cytometry incorporating fluorescence lifetime measurements could significantly improve the
42 throughput, advancing applications to biological and biomedical research such as directed
43 evolution of FPs¹⁹, protein subcellular localization²⁰, protein-protein interaction²¹, drug
44 discovery²², and cellular physiology^{23,24}.

45
46 Lifetime-based flow cytometry has been demonstrated at a sorting throughput of hundreds of cells
47 per second.²⁵ However, there are limitations associated with fluorescence detection in a continuous
48 flow stream. For cellular applications, it restricts the fluorescent markers and reactions to be inside
49 or on the cellular surface and is limited to applications that are insensitive to inter-cellular
50 interactions. One approach for overcoming these limitations is to encapsulate cells or other
51 analytes into isolated droplets that retain their integrity throughout the analysis, and sorting. The
52 ease with which stable droplets can be formed with pL-scale, tunable volumes makes droplet
53 microfluidics particularly useful for analyzing individual molecules, cells or other discrete analytes
54 such as beads. These capabilities has been utilized for studying enzymatic activity *in cellulo*^{26,27}
55 and *in vitro*²⁸, single-cell analysis and sorting²⁹, screening for antibiotic resistance^{30,31}, directed
56 evolution of enzymes³², genetically-encoded biosensors^{33,34}, and quantifying heterogeneity at the
57 single cell level^{35,36}. Moreover, microfluidic droplet platforms can be designed for novel flow
58 cytometry applications such as those simultaneously requiring temporally well-defined mixing of
59 cells with reagents followed by time-resolved detection. Fiedler and coworkers have demonstrated
60 resolution and sorting of genetically-encoded biosensors based on various Förster Resonance
61 Energy Transfer (FRET) ratios measured with delay time in seconds³⁴. The same platform can be
62 readily modified for directed evolution of fluorescent proteins or enzymes.

63
64 The throughput of lifetime-based droplet sorters is impacted by a number of factors. First, the
65 statistics of cell loading into droplets typically follows the Poisson distribution³⁷. To ensure single
66 cell loading, the proportion of non-empty droplets is often limited to < 10% of the whole droplet
67 population. Unfortunately, this sparse loading limits the throughput and is therefore often regarded
68 as a disadvantage of the droplet platform. Deterministic single cell encapsulation methods
69 overcome the limitation imposed by Poisson statistics, but there are other limitations such as
70 increased device complexity, substantial proportion of unsorted or wrongly selected droplets, and
71 high flow rates, which limit the flexibility of integration with other systems³⁸. Second, the
72 throughput of a conventional droplet sorter is limited to 2~3 kHz due to the use of a hard divider
73 to separate the collection and waste channels, but new geometries have been investigated to surpass
74 this limitation achieving brightness-based sorting at 30 kHz³⁹. Finally, fast data processing of
75 fluorescence lifetime signatures and real-time sorting decision and actuation components are
76 crucial for achieving kHz sorting rates. Despite advances in incorporating fluorescence lifetime
77 measurements into droplet selection methods, the throughput is much lower than purely
78 brightness-based droplet sorting. For example, the throughput of a recently reported fluorescence
79 lifetime droplet microfluidic sorter is 50 droplets/s⁴⁰. A FACS enrichment step is often used to
80 enrich a subset of targets from a large pool prior to selection or investigation on other parameters
81 and platforms^{19,41-43}. Performing fluorescence lifetime selection with this combination of methods
82 is disadvantageous. In addition to the restrictions imposed by a continuous flow stream in the
83 FACS step, the use of two different instruments imposes uncertainties into the overall selection
84 because the fluorescence intensity values are difficult to calibrate between instruments.

85
86 Within the general realm of sorting applications, the analysis, enrichment, and isolation of rare
87 macromolecules, cells and particles from a large population constitutes an important subset that is
88 of great importance across a broad area of biomedical, biotechnological, and environmental
89 science. Several papers have described approaches to this challenge in which a rare population is
90 analyzed without isolating it, or where an initial enrichment is advantageous compared to one-

91 step, single-particle isolation. For example, fluorescence brightness-based droplet digital detection
92 has been applied to the detection of single bacteria in unprocessed blood⁴⁴ and profiling circulating
93 tumor DNA,⁴⁵ and the implementation of fluorescence lifetime detection was demonstrated to
94 increase the specificity of particle counting⁴⁶. An ensemble sorting approach which repeatedly
95 analyzes and sorts batches within a sample was recently proposed for enriching or separate
96 fluorescent particles⁴⁷. Many microfluidic systems have been developed to enrich and isolate
97 circulating tumor cells, as reviewed in reference 48. Here, we quantify the advantages of a batch
98 sorting technique for increasing the throughput of rare-clone isolation.

99
100 In this work, we have developed a multiparameter high throughput water in oil droplet microfluidic
101 sorter capable of screening and sorting analytes based on emission spectra, emission brightness,
102 and fluorescence lifetime. We raised the throughput of lifetime sorting to the upper limit possible
103 for a droplet sorter with a hard divider between collection and waste channels³⁹. This performance
104 constitutes a 50-fold increase compared to a recently reported lifetime droplet sorter⁴⁰. We also
105 describe and demonstrate a novel selection strategy, similar to an ensemble-based approach, which
106 exploits the Poisson statistics of analytes in droplets overloaded with multiple analytes. This
107 method provides a several-fold enhancement in sorting throughput. The strategy can be used to
108 analyze and enrich rare events from a large population in either a qualitative manner without prior
109 knowledge for the initial frequency of the rare events, or in a quantitative fashion with controls of
110 the efficiency and precision of enrichment when the initial frequency of the rare events is estimated.
111 The enriched sub-population can be subjected to further multiparameter analysis and selection with
112 single-cell resolution on the same microfluidic platform. We demonstrate the power of this
113 multiparameter droplet sorter and the enrichment strategy in the context of directed evolution of
114 red fluorescent proteins (RFPs) expressed in *E. coli*.

115

116 **Experimental**

117

118 *Optical Layout*

119

120 The optical layout of the instrument is depicted in Section 1 of Supplementary Information. Both
121 561 nm and 450 nm continuous wave (CW) laser beams excite fluorescence from the cells
122 encapsulated in droplets. The 561 nm beam is focused into an electro-optic modulator that can
123 amplitude modulate the CW beam to a sinusoidal profile. The red and green fluorescence signals
124 are separated by a dichroic mirror and detected by photomultiplier tubes (PMTs).

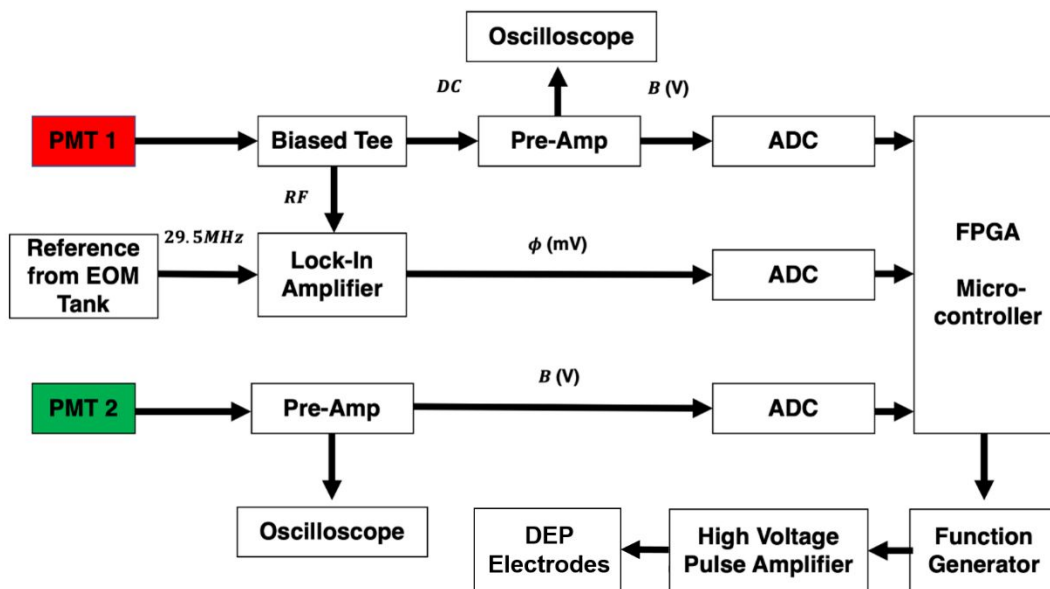
125

126 *Electronics and microfluidic device*

127

128 The main improvement of sorting throughput in this work is due to the implementation of faster
129 electronics. The layout of the detection electronics is schematically described in Figure 1. The
130 electro-optic modulator (EOM; ThorLabs EO-AM-NR-C4) is used to modulate the 561 nm laser
131 light and is driven using a function generator (Agilent 33520B) that provides a 1 V peak to peak
132 sinusoidal signal at 29.5MHz to a resonator circuit. When screening or sorting based on
133 fluorescence lifetime, the red fluorescence signals from PMT1 are separated into a radio frequency
134 (RF) component (that bears the lifetime information) and the direct current (DC, <83KHz)
135 component using a bias tee. To improve the signal to noise ratio, the DC signals from the biased-
136 tee and from PMT2 (green fluorescence) are amplified using home-built trans-impedance log or

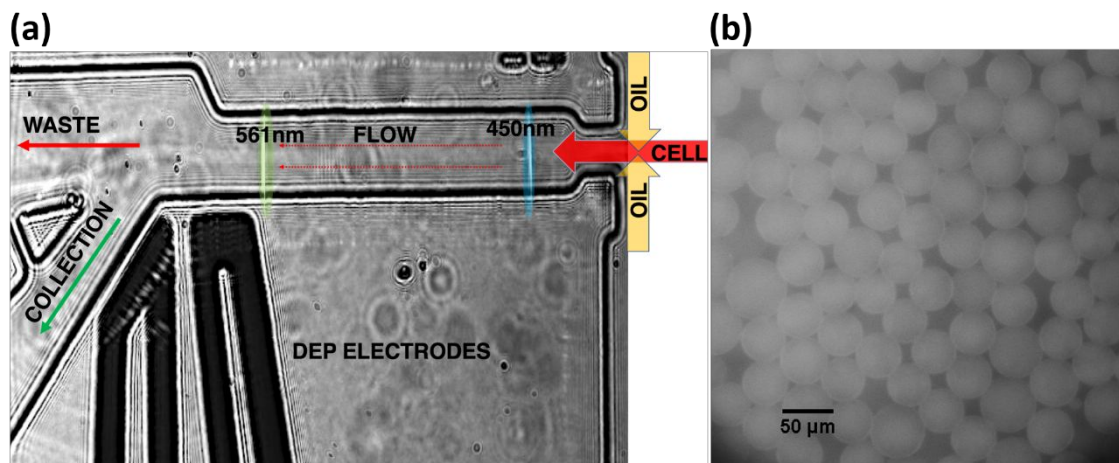
137 linear pre-amplifiers, depending upon the experiment and sample in use¹⁹, then digitized using
 138 Analog to Digital Converter (ADC) boards (Analog Devices, EVAL-AD7986FMCZ, 18 bit). The
 139 RF component of the signal is passed onto a commercial high-speed lock-in amplifier (Zurich
 140 Instruments UHFLI), which calculates the phase shift of the fluorescence signal relative to the
 141 sinusoidal modulation signal to extract information of fluorescence lifetime. The phase shift value
 142 from the lock-in amplifier is then digitized using the same type of ADC boards employed for
 143 brightness measurements. The digitized signals from the boards are then fed into a customized
 144 field programmable gate array (FPGA) board that makes decisions based on user defined
 145 parameters interfaced through a LabView program. Use of an FPGA has been demonstrated to
 146 enhance the data processing rate for fluorescence lifetime calculation.⁴⁹ Brightness and lifetime
 147 signals from encapsulated cells in droplets that fulfil the selection criteria are then sorted using
 148 dielectrophoresis (DEP) technique.³⁴ The FPGA sends a sort signal to trigger a function generator
 149 (Keysight 33509B) which provides a square wave pulse which is amplified 1000x in a high voltage
 150 amplifier (TREK), before being sent to the electrodes of the microfluidic device. The flow is biased
 151 towards the waste channel, so droplets are only directed to the collection channel when the FPGA
 152 sends a signal to trigger a high voltage pulse to DEP electrodes. The fluorescence detection and
 153 cell selection regions of the device are shown in Figure 2(a). Further details on the microfluidic
 154 device are provided in Section 1 of Supplementary Information.



155

156 **Figure 1:** Schematic layout of the electronics used in this sorter.

157



158

159 **Figure 2:** (a) Camera image shows the typical droplet flow with both excitation beams on. The
 160 microfluidic chip is designed such that droplets are biased towards the waste channel. (b) Image
 161 of droplets containing Rhodamine B generated with the microfluidic chip. The scale bar indicates
 162 50 μm .

163

164 *Instrument operation*

165

166 The microfluidic sorter is configured with excitation beams at 450 nm and 561 nm, wavelengths
 167 which allow for screening based on green and/or red fluorescence signals respectively. The 561
 168 nm excitation beam is modulated at 29.5 MHz, enabling fluorescence lifetime screening in the red
 169 channel. To count the number of droplets passing each channel and monitor the flow (number of
 170 droplets per second) throughout an experiment, the laser intensities and PMT voltages were set
 171 such that a small portion of scattered laser light from each droplet bleeds through the dichroic
 172 mirror and the emission filters and can be detected in both channels. We previously reported
 173 fluorescence lifetime sorting in a microfluidic flow cytometer, however, the sorting speed was
 174 limited to ~ 30 cells/s because communication among instruments, target and host computers,
 175 calculation of fluorescence phase shifts, and sorting decisions relied on software developed on a
 176 LabView¹⁹ platform. In the current sorter, the phase shifts are obtained directly from a high-speed
 177 lock-in amplifier, and an FPGA coordinates communication among all electronics and performs
 178 sorting decisions. A LabView user interface is designed only for setting selection parameters,
 179 acquiring data from the FPGA and real time plotting. As a result, the new instrument operates at
 180 ~ 100 -fold higher screening and sorting speeds. For both fluorescence-activated droplet sorting
 181 (“brightness sorting”) and fluorescence lifetime-activated droplet sorting (“lifetime sorting”), the
 182 FPGA and Labview program are designed such that the sorting thresholds can be set to exclude
 183 empty and unwanted droplets for sorting purposes, while counting the total number of droplets and
 184 monitoring the flow (number of droplets per second). Both brightness and lifetime measurements
 185 have been tested at droplet generation rates up to 4 KHz (~ 0.7 mL/hr volumetric flow rate) for
 186 screening and 2.5 kHz (~ 0.45 mL/hr volumetric flow rate) for sorting. A typical image of droplets
 187 generated at ~ 2.5 kHz (Figure 2(b)), demonstrates their size uniformity and agreement with the
 188 estimated droplet volume ~ 50 pL which is determined from the droplet generation rate and the
 189 0.45 mL/hr volumetric flow rate. More details about instrument operation are supplied in Section
 190 2 of the Supplementary Information.

191

192 Cell culture and sample preparation

193

194 The droplet microfluidic sorter can be employed to assay diverse cell types, such as bacteria,
195 phytoplankton, yeast, and mammalian cell lines. To test the performance of this sorter, various FPs
196 with distinct fluorescence lifetime, brightness, and spectra were expressed in *E. coli*. Cells
197 expressing FPs were prepared at desired concentrations according to the measurement
198 of their optical density (OD) and connected to the aqueous inlet of the microfluidic chip.
199 The details of cell culture and sample preparation are described in Section 3 of
200 Supplementary Information.

201

202 Results and Discussion

203

204 This instrument control software is designed such that one can choose the desired combinations of
205 screening and/or sorting based on emission spectrum, brightness, and red fluorescence lifetime.
206 The scattered excitation light from each droplet can be detected by the PMTs, which allows us to
207 monitor the flow, count the number of droplets, and pair-match two events in green and red
208 channels for a particular droplet. Details of data acquisition and signal processing are described in
209 Section 4 of Supplementary Information. The performance of brightness and lifetime sorting with
210 different screening/sorting criteria is evaluated here. We also present some examples of the
211 strategy for enriching rare events with multiple cell encapsulation.

212

213 Performance of two-color brightness-sorting

214

215 To evaluate the performance of brightness detection in the green and red channels, *E. coli* cells
216 expressing EGFP and mScarlet were screened respectively to find the mean brightness in each
217 channel. An approximately 1:1 mixture was prepared and droplets with a brightness threshold
218 greater than mean brightness in the red channel were sorted to select mScarlet from $\sim 10^5$ droplets.
219 The sorted cells were subsequently grown overnight and screened 16 hours after induction of
220 expression to evaluate the sorting efficiency. All screening and sorting experiments were
221 performed at a rate of 2 kHz with an average cell concentration of 0.1 cell/droplet, where 9.5% of
222 the droplets are filled and 95% of filled droplets contain a single cell. The results shown in Section
223 5 of Supplementary Information reveal a sorting efficiency of $86 \pm 1\%$ averaged from 3
224 experimental trials, i.e. 86% of re-grown cells have mScarlet and 14% of them have EGFP in
225 average. The 14% re-grown cells expressing EGFP reflects several factors including the 5% of
226 filled droplets containing multiple cells, varying cytotoxicity for cells expressing different FPs⁵⁰,
227 and the excitation conditions. These issues are discussed in the lifetime sorting section, below.

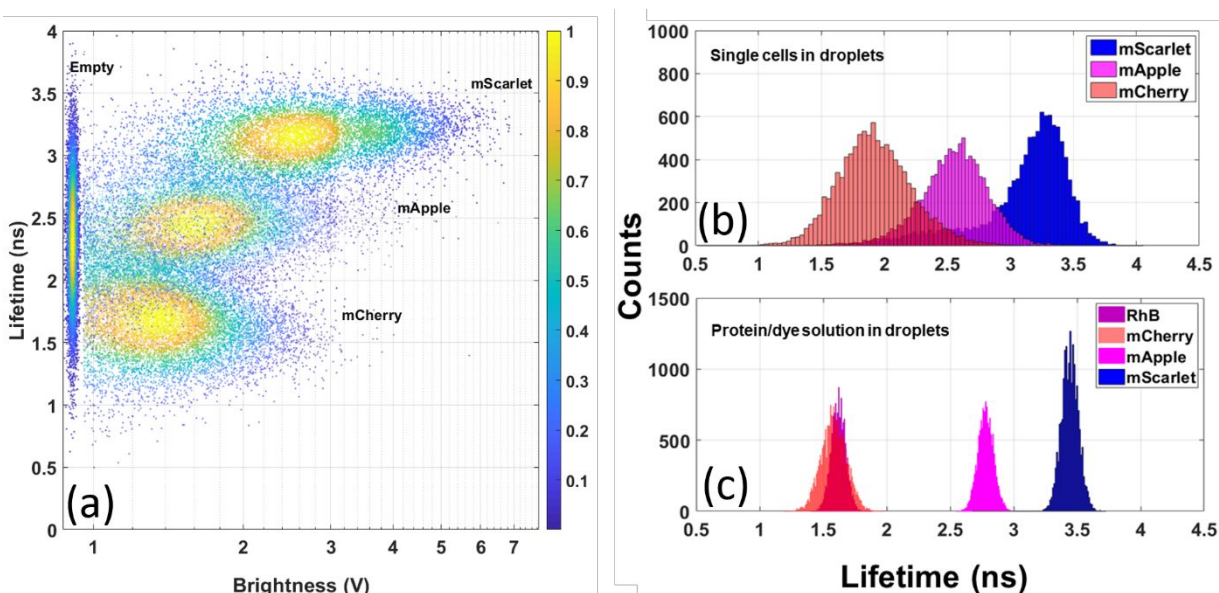
228

229 Performance of lifetime sorting

230

231 The phase shift measured in the frequency domain technique is sensitive to the modulation
232 frequency⁵¹, transit time of cells passing through the laser beam, and settings of the PMT and lock-
233 in amplifier. Determination of the lifetime and its dependence on these experimental factors is
234 described in Section 4 of Supplementary Information. *E. coli* cells expressing mCherry, mApple,
235 or mScarlet were screened with brightness and lifetime at a rate of 2.5 kHz. The major population
236 of each RFP is distinguishable by its fluorescence lifetime as shown in Figure 3(a). The results

237 reveal heterogeneity in both fluorescence brightness and lifetime, as observed in our previous work
 238 on other RFPs¹⁹. The spread of lifetime values is about 0.5-1 ns for these RFPs at full width at half
 239 maximum (FWHM) of the histograms in Figure 3(b).
 240



241 **Figure 3:** (a) Fluorescence lifetime and brightness plots of empty droplets and individual RFPs
 242 expressed in *E. coli* screened sequentially (10^4 cells each). Pseudocolor indicates the normalized
 243 cell counts with a particular bin of fluorescence lifetime and brightness on the plot, ranging from
 244 yellow for the highest to indigo indicating the lowest counts. The mean fluorescence lifetime is
 245 1.7 ns (set as reference), 2.6 ns, and 3.3 ns for mCherry, mApple, and mScarlet respectively. (b)
 246 Corresponding fluorescence lifetime histograms. (c) Fluorescence lifetime histograms of
 247 Rhodamine B (RhB) and three purified proteins measured in the microfluidic sorter. The mean
 248 fluorescence lifetime is 1.6 ns (set as reference), 1.6 ns, 2.8 ns, and 3.5 ns for RhB, mCherry,
 249 mApple, and mScarlet respectively.
 250

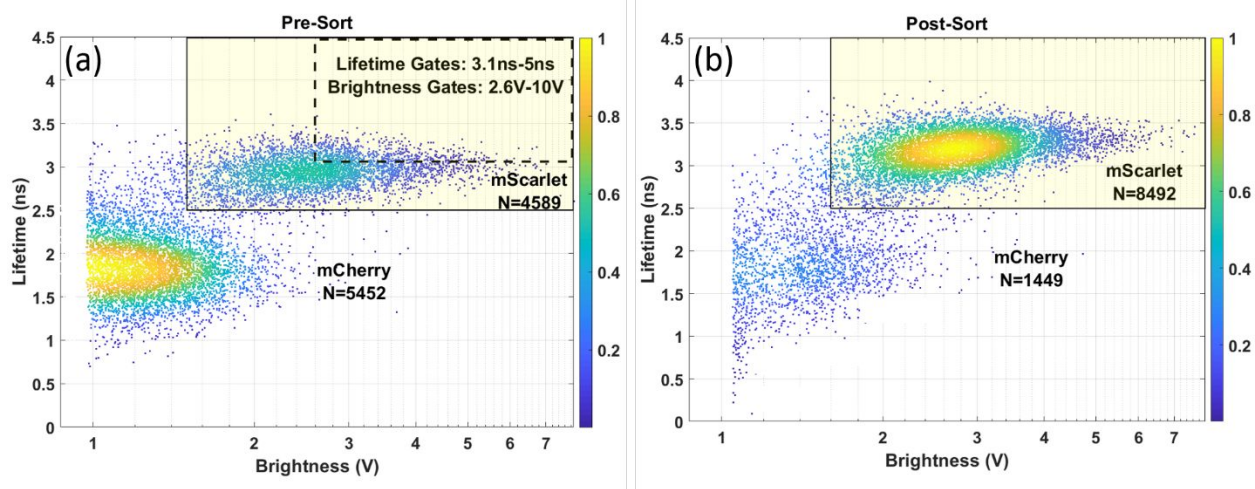
251 The asymmetric histograms of fluorescence lifetime in Figure 3(b) can be understood as an effect
 252 resulting from the contribution of scattered excitation light detected along with the fluorescence
 253 signal. This effect is modeled with a simulation in Section 4 of the Supplementary Information.
 254 Ideally, scattered light has a constant phase shift (which is converted to the fluorescence lifetime)
 255 relative to the modulated laser beam due to optical and electronic delays. This is included in the
 256 total phase shift by setting the reference phase shift of a bacterial colony expressing mCherry on a
 257 plate to 45 degrees. In this particular experiment, the total offset phase shift of empty droplets
 258 corresponds to a fluorescence lifetime centered on ~ 2.35 ns with a wide distribution due to low
 259 signal-to-noise ratio (SNR). The scattered light is added to the fluorescence signal and both signals
 260 have the same modulation frequency but different phase shift values, so the lock-in amplifier
 261 extracts an averaged phase value from the combined signals. The influence of scattered light is
 262 more significant at low fluorescence brightness, whereas the average lifetime value approaches the
 263 actual fluorescence lifetime value as the fluorescence brightness increases.
 264

265 The distribution of lifetime measured from a single-FP population can be attributed to cellular
 266 heterogeneity, excitation condition and electronics. Cellular heterogeneity is an intrinsic
 267 biochemical property that can only be resolved in single cell analysis methods such as this

268 microfluidic droplet sorter. On the other hand, the noise originating from the excitation condition
269 may be further reduced. The diameter of the droplet is estimated to be $\sim 46 \mu\text{m}$, but the Rayleigh
270 length of the excitation beam is $\sim 10 \mu\text{m}$, hence the location of the cell inside a droplet could lead
271 to variations in fluorescence brightness resulting in uncertainties in lifetime measurement.
272 Theoretically the lifetime is independent of fluorescence signal level, but in practice the scattered
273 excitation light affects weaker fluorescence signals more than stronger ones as discussed above.
274 We further investigated the spread of lifetime due to electronics by performing *in vitro*
275 measurements. In addition to eliminating the cellular heterogeneity, *in vitro* measurements also
276 minimize the fluctuations from excitation condition since a droplet has homogeneous fluorophore
277 concentration and the Rayleigh length is always within the droplet. It is worth noting that various
278 *in vitro* assays can be performed with a droplet platform, but it is difficult to perform them with a
279 continuous stream cytometry. Three purified proteins, mCherry, mApple, and mScarlet, and an
280 organic dye, Rhodamine B, were screened for fluorescence lifetime using the sorter. The histogram
281 of fluorescence lifetime is shown in Figure 3(c), with FWHM $\sim 0.1 \text{ ns}$ for Rhodamine B and ~ 0.2 -
282 0.3 ns for FPs. The wide spread in lifetime for mCherry is likely due to its low SNR resulting from
283 a low quantum yield (hence low molecular brightness). Nonetheless, the FWHM of fluorescence
284 lifetime measured from an *in vitro* experiment is much narrower than that from a cellular
285 measurement. The result indicates that the uncertainty originating from electronics is significantly
286 less than other sources. This also suggests that the lifetime resolution for cellular screening could
287 be improved by reducing the droplet size and/or expanding the beam size to extend the Rayleigh
288 length to ensure that the encapsulated cells are within the Rayleigh length, i.e. an improved uniform
289 excitation condition. This effect will be reduced with larger cell types such as yeast or mammalian
290 cells. Finally, note that the disagreement in the average lifetime among cellular and *in vitro*
291 measurements suggests that the cellular environment differs from the *in vitro* environment. For
292 example, fluorescence lifetime of FPs varying with environmental pH^{5,6} and refractive index^{7,8} has
293 been reported and used for sensing and imaging applications. Details of the *in vitro* experiment
294 including the comparison of fluorescence lifetime measured using the sorter and Time-Correlated
295 Single Photon Counting (TCSPC) are described in Section 5 of Supplementary Information.

296
297 To demonstrate the performance of lifetime-based sorting, *E. coli* cells expressing mScarlet or
298 mCherry were mixed in a $\sim 1:1$ proportion and sorted at 2.5 kHz with two parameters, fluorescence
299 lifetime and brightness, at an average concentration of 0.1 cell/droplet . This sort rate represents
300 the fastest fluorescence lifetime droplet sorting reported to date. Approximately 3×10^3 droplets
301 were sorted from $\sim 2.5 \times 10^5$ droplets with the selection gates set to the mean brightness value and
302 mean fluorescence lifetime of mScarlet. The sorted cells were subsequently grown, expressed for
303 16 hours and re-screened to evaluate the sorting efficiency. The screening results before and after
304 sorting are shown in Figure 4, demonstrating an 85% sorting efficiency. The experiment was
305 additionally repeated 3 times with a new mixture, sorting mScarlet or mCherry, and the average
306 efficiencies were $80 \pm 1\%$ and $97 \pm 1\%$ respectively, as described in Section 5 of Supplementary
307 Information. The discrepancy between sorting mScarlet and mCherry can be attributed to the
308 process of re-growing and expressing enriched cells in the experiment with the assumption that
309 bacteria expressing different FPs have the same growth rate, which may not be accurate. Some
310 mCherry mutants, mApple, and EGFP have been reported to show a range of cytotoxicities when
311 expressed in *E. coli*⁵⁰. The difference between two batches of mScarlet enrichment experiments
312 may be due to the flow condition, the biological variation (two biological duplicates in two batches

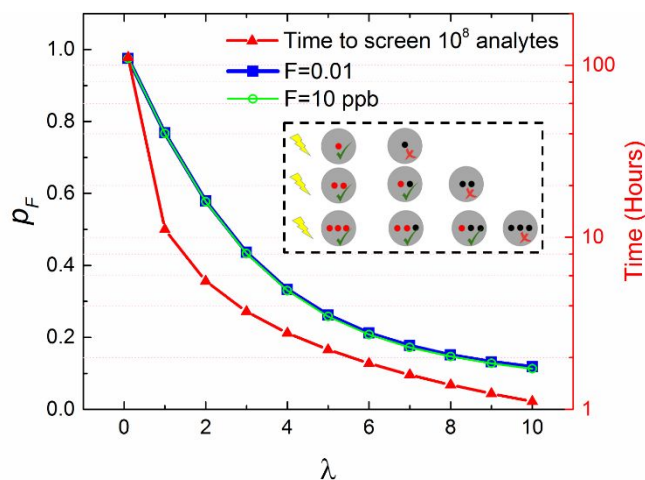
313 of experiments) and the uncertainty of cell concentration in the sample preparation causing
 314 variations in λ , which affects the sorting efficiency that will be further discussed below.
 315



316
 317 **Figure 4:** Fluorescence lifetime versus brightness scatter plots of mixed cells before and after
 318 sorting. Solid boxes indicate the thresholds for counting cells expressing mScarlet. N is the number
 319 of cells expressing each RFP. (a) Mixture of *E. coli* cells expressing mCherry and mScarlet before
 320 sorting. The dashed box indicates the two-parameter sorting gates. (b) Screening results after
 321 sorted cells were grown overnight and expressed for 16 hours. The brightness threshold was set
 322 slightly higher than pre-sort to exclude the stronger scattered excitation signals from droplets in
 323 the post-sort screening, because changing microfluidic chips introduces variations in the focus of
 324 the excitation beam and thus the amount of scattered light.

325 *Strategy for enriching rare fluorescent events*

326
 327 For a large library containing rare events, the overall throughput can be greatly increased by sorting
 328 droplets by encapsulating multiple cells in a single droplet as an initial round of enrichment. The
 329 efficiency of this strategy can be estimated by considering the Poisson distribution, the
 330 combination of cells resulting fluorescent droplets, and the percentages of fluorescent cells in a
 331 library. Consider the combination of cells encapsulated in droplets is illustrated in the inset of
 332 Figure 5. A droplet will be detected with fluorescence as long as it contains one or more fluorescent
 333 cells. The probability of number of cells (N) encapsulated in a droplet is $\text{Prob}(N) = (e^{-\lambda} \times \lambda^N) / N!$,
 334 where λ is the average number of cells per droplet.
 335



336
 337 **Figure 5:** The efficiency of enrichment with various initial fraction of target analyte (cells,
 338 molecules, or beads) and the required enrichment time as a function of average number of cells
 339 per droplet. Inset (dashed box): Illustration of cells encapsulated in droplets. The red and black
 340 dots indicate fluorescent and non-fluorescent cells, respectively. The green check and red cross
 341 marks indicate fluorescent and non-fluorescent droplets.

342
 343 Assuming a library with initial fraction F of fluorescent cells, the probability of finding fluorescent
 344 cells after sorting, p_F , is

$$345 \quad p_F = \sum_{n=1}^{\infty} \frac{\sum_{i=1}^n \binom{n}{i} \cdot i \cdot F^i \cdot (1-F)^{n-i}}{n \cdot \sum_{i=1}^n \binom{n}{i} \cdot F^i \cdot (1-F)^{n-i}},$$

346 where i is the number of fluorescent cells and n is the number of cells per droplet. Since the
 347 probability of encapsulated cells per droplet decreases quickly with the increasing number of
 348 encapsulated cells, the p_F can be numerically calculated using $n \leq 50$ for $\lambda \leq 10$. The Poisson
 349 distribution for $\lambda \leq 10$ is plotted in Section 6 of Supplementary Information. The efficiency of the
 350 multiple-cell encapsulation enrichment, which is indicated by the improvement in the fraction of
 351 fluorescent cells after sorting (i.e. p_F), is estimated with $F=0.01$ and $F=10$ ppb for various λ as
 352 shown in Figure 5. The results indicate that with one round of sorting, the fluorescent cells in the
 353 library can be enriched to about the same fraction regardless of the initial fraction F , thus this
 354 selection strategy is more powerful for enriching rarer events from a large pool (i.e. small F). It is
 355 not surprising that the enrichment efficiency is significantly affected by the average number of
 356 cells per droplet (λ), but the influence from the fraction of fluorescent cells in the original library
 357 is not significant, because the selected droplets all contain fluorescent cells. Assuming a sorting
 358 speed of 2.5 kHz, the time required for screening 10^8 cells as a function of λ is plotted in Figure 5.
 359 The result clearly shows that the time can be drastically reduced by including multiple cells in a
 360 droplet. The estimation of p_F only considers the statistical probability, i.e. the number of screened
 361 cells is much larger than the inverse of the initial fraction F . Such enrichment efficiency, p_F , is
 362 estimated to hold for enriching ≥ 0.5 ppm targets from 10^8 cells, the limit for current throughput to
 363 complete enrichment in a few hours without losing cell viability, in Section 6 of Supplementary
 364 Information. However, this does not limit the application of the enrichment strategy from sorting
 365 smaller fraction of rare events. With smaller fraction of rare events, the enrichment efficiency may

366 deviate from the expected value plotted in Figure 5, but it still provides approximately the same
367 order of magnitude of enrichment efficiency as illustrated in Section 6 of Supplementary
368 Information.

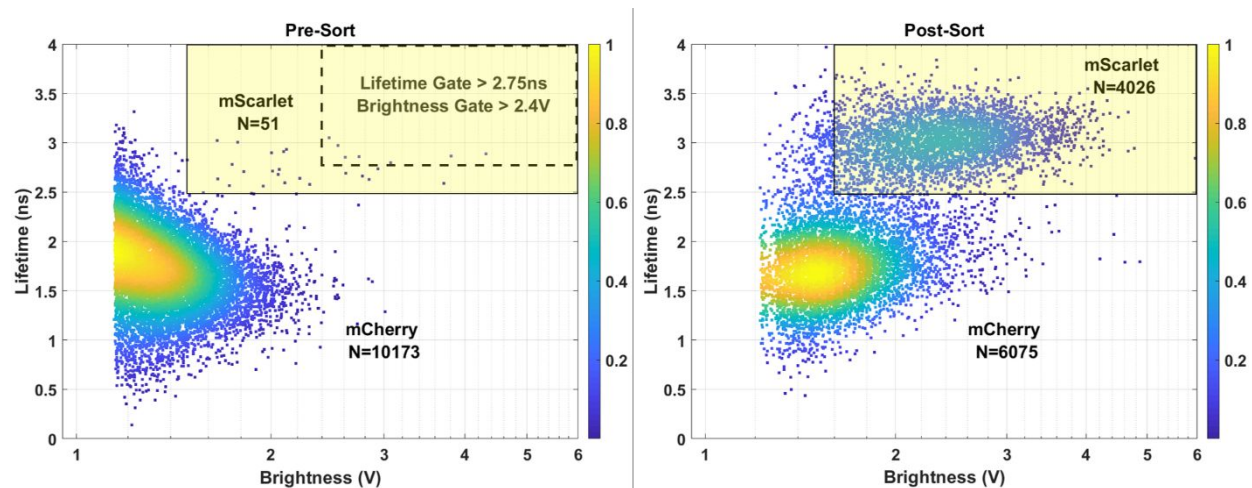
369
370 To further illustrate the power of this enrichment strategy, we consider two examples of rare events
371 that fluoresce or exhibit a distinct fluorescence lifetime relative to the main fluorescent population.
372 Assume the enrichment is carried out with brightness or lifetime sorting operating at 2.5 kHz with
373 an average 4 cells/droplet encapsulation. In the first example, we assume that the fraction of the
374 rare events is 1 ppm. It would take less than 3 hours to enrich rare events from a 10^8 population,
375 resulting in a subset of 100 fluorescent cells mixed with 203 unwanted cells ($p_F=0.33$), i.e.
376 3.3×10^5 -fold enrichment (p_F/F) in one round of sorting. The enriched subset can be further cultured,
377 analyzed, or sorted with single cell resolution to isolate the final, purified population. In the second
378 example, we consider a cell-based library containing 33×10^6 distinct mutants. To ensure the
379 enrichment covers 95% of this library, at least 3 times of the library size must be screened⁵², which
380 is $\sim 10^8$ cells. Assuming the desired clones comprise 1% of the original library, this enrichment
381 reduces the library size from 33×10^6 down to 1×10^6 within 3 hours with 0.33×10^6 fluorescent cells,
382 thus a 33-fold enrichment. The enriched library can be further analyzed or sorted at $\lambda=0.1$ (single-
383 cell resolution) using brightness or lifetime sorting. Using the conventional encapsulation strategy
384 ($\lambda=0.1$) without the enrichment, it would take ~ 117 hours to complete the selection in both
385 examples with brightness or lifetime sorting at the speed of 2.5 kHz developed in this work. It
386 would take 50 times longer (~ 5848 hours) for a recently reported lifetime droplet sorting⁴⁰ to
387 perform the selection. Using a state-of-the-art droplet sorting at 30 kHz³⁹, the selection would
388 require ~ 10 hours, which is more than 3 times longer than the lifetime enrichment demonstrated
389 here, to complete a brightness-only selection in single cell resolution without fluorescence lifetime
390 information. The combination of this new sorting technology and enrichment strategy enables fast
391 multiparameter analysis and selection of rare events from a 10^8 -member population based on
392 fluorescence lifetime, brightness, and spectrum, as a preparation for further investigation and
393 sorting with single cell resolution on a single instrument.

394
395 To demonstrate the effectiveness of this strategy, we enriched mScarlet from a mixture of EGFP
396 and mScarlet transformed in *E. coli* using dual color brightness sorting. Since EGFP does not emit
397 red fluorescence, EGFP can be regarded as the non-fluorescent population and mScarlet as the rare
398 fluorescent population observed in the red channel. The number of EGFP cells can be counted in
399 the green channel since only EGFP contributes to the green emission. Thus, the fraction of
400 mScarlet (i.e. the fluorescent events in the red channel) in the mixture was determined to be $F \sim 0.01$.
401 After one round of enrichment with $\lambda=3$ encapsulation, the sorted cells were subsequently grown,
402 expressed and screened with $\lambda \leq 0.1$ encapsulation. The mScarlet population was enriched to an
403 average $35 \pm 4\%$, which agrees with the expected value ($p_F \times 0.86$) $\sim 37\%$, taking into account the
404 86% efficiency of single cell two-color sorting described earlier. The experimental details can be
405 found in Section 6 of Supplementary Information.

406
407 The enrichment strategy can also be applied in lifetime sorting when the rare events have a distinct
408 fluorescence lifetime from the major population, despite the overlap in emission spectra and
409 brightness. We demonstrate the enrichment of rare cells expressed with mScarlet from a mixture
410 of mCherry and mScarlet, which have large overlap in both emission spectra and cellular
411 brightness. The first test was carried out the same day using the same batch of sample generating

412 results in Figure 4. The fraction of mScarlet in the mixture before enrichment was estimated to be
 413 $F \sim 5 \times 10^{-3}$. The enrichment was performed with $\lambda=3$ at 2.5 kHz, and the sorted cells were
 414 subsequently grown, expressed and screened with $\lambda \leq 0.1$. We attained an enrichment of the
 415 mScarlet population to 40% (Figure 6), which is consistent with the expected value, including the
 416 85% efficiency of single cell lifetime sorting demonstrated in Figure 4, $(p_F \times 0.85) \sim 37\%$. Another
 417 enrichment for rare mScarlet was performed using the second batch of sample with $F \sim 5 \times 10^{-3}$,
 418 resulting in an average enrichment of the mScarlet population $30 \pm 5\%$, in agreement with the
 419 expectation $(p_F \times 0.80) \sim 35\%$. Experimental details are described in Section 6 of Supplementary
 420 Information.

421



422

423 **Figure 6:** Fluorescence lifetime versus brightness scatter plots of rare mScarlet enrichment. Solid
 424 boxes illustrate thresholds for counting cells expressing mScarlet. N is the number of cells
 425 expressing each RFP. (Left) Mixture of *E. coli* cells expressing mCherry and mScarlet before
 426 enrichment. The dashed box indicates the two-parameter sorting gates. (Right) Screening results
 427 after enriched cells were grown overnight and expressed for 16 hours.

428

429 *Enrichment of an RFP library*

430

431 The directed evolution of FPs often involves the screening of cell libraries with rare bright clones.
 432 Library size increases exponentially with the number of target residues, and FP libraries are
 433 typically found to have a narrow fitness landscape⁵³, i.e. the fraction of fluorescent clones
 434 dramatically decreases as the mutational space increases due to protein mis-folding, incomplete
 435 chromophore maturation, and other photophysical factors. We used this sorter to enrich the
 436 population of fluorescent RFP mutants and select the brightest ones for further development.
 437 Taking mScarlet-I as the template, we constructed a site-directed library with the size $\sim 1.7 \times 10^7$,
 438 which requires screening $> 5.1 \times 10^7$ cells to cover 95% of the library size. In our previous studies
 439 of site-directed and/or error-prone PCR libraries of red FPs (RFPs), some non-fluorescent colonies
 440 were observed to grow larger than fluorescent ones on plates, likely due to variations in
 441 cytotoxicity of various mutations in RFPs⁵⁰. Therefore, we expect reduced sorting efficiency due
 442 to the re-growth and expression processes after enrichment as described above. With this
 443 consideration in mind, we decided to load the droplets with $\lambda=3$, and a total number of $\sim 8 \times 10^7$ *E.*
 444 *coli* cells expressing this RFP library was screened in two batches (ensuring the health of cells) to

445 enrich fluorescent cells at ~ 2 kHz. The proportion of fluorescent cells was enriched from initially
446 $\sim 5\%$ to $\sim 30\%$. This is lower than the expected, empirically corrected enrichment efficiency
447 ($43\% \times 0.86$) 37% for $\lambda=3$. The enriched population underwent 3 more rounds of enrichments with
448 higher thresholds in fluorescent brightness with $\lambda=1$ or $\lambda=0.1$ at 2 kHz, resulting in $>95\%$
449 fluorescent population. The final round of sorted cells was re-grown overnight then expressed on
450 agar plates. Three distinct mutants were identified from the agar plates for further development.
451 More information on the library and the detailed enrichment procedure are provided in Section 7
452 of Supplementary Information.

453
454 This platform is sufficiently flexible to support further enhancements. For example, additional
455 excitation wavelengths with RF modulation can be implemented to expand the information content
456 in both spectral and fluorescence lifetime dimensions. Furthermore, it is possible to increase the
457 sorting speed further by modifying the microfluidic chip design. In particular, brightness sorting
458 at 30 kHz has been demonstrated in a design where the hard divider is replaced with a gapped
459 divider to separate outlets³⁹. In addition, increasing the modulation frequency of the excitation
460 beam shortens the phase acquisition time, and therefore increases the fluorescence lifetime
461 detection speed. As such, a modulation frequency of 100 MHz could support a ~ 3.4 -fold increase
462 in sorting speed. However, the modulation frequency may set the limit for the throughput of
463 fluorescence lifetime measurement. When the modulation frequency increases to higher than 100
464 MHz, the period of the modulation wave becomes less than 10 ns, the same order of magnitude as
465 the fluorescence lifetime of commonly used fluorophores. This may disturb the phase
466 measurement under a strong excitation rate used in frequency domain measurement. On the other
467 hand, to further increase the sorting speed to ≥ 10 kHz, the adjoining scattering or fluorescence
468 signals are ≤ 100 μs apart. In current setup, the FWHM of the scattering and fluorescence signals
469 is approximately 25 μs at 2 kHz, which is sufficiently small for sorting at 10 kHz. If needed,
470 decreasing the droplet size can not only reduce the noise as previously discussed, but also shorten
471 the transient time of the droplet and cells since they only pass the Rayleigh length region, resulting
472 in narrower FWHM of the scattering and fluorescence signals. Thus, it is feasible to improve the
473 throughput of this multiparameter droplet sorter to ≥ 10 kHz.

474 475 **Conclusion**

476
477 A multiparameter microfluidic droplet sorter combining the detection of fluorescence lifetime,
478 brightness, and spectrum has been developed in this work. The throughput of the fluorescence
479 lifetime measurement and sorting, up to 4 kHz for screening and 2.5 kHz for sorting with current
480 chip design, is greatly enhanced by using a FPGA for the communication among all electronics
481 and sorting decisions. To our knowledge, this is the fastest fluorescence lifetime droplet screening
482 and sorting speed to date. The high-throughput fluorescence lifetime droplet sorting opens the
483 opportunity of integrating fluorescence lifetime detection with other high throughput detection
484 methods in a microfluidic droplet platform to increase the information content of biological and
485 biomedical assays with single cell resolution.

486
487 We have also proposed a novel multiple-cell encapsulation strategy enriching the rare events to
488 overcome the obstacle of droplet sorting throughput limited by the nature of Poisson distribution
489 for random cell/molecule encapsulation – by taking the advantage of Poisson statistics. The effect
490 of enrichment increases tremendously as the fraction of rare events decreases. The efficiency and

491 precision of enrichment can be quantitatively controlled if the rare event frequency is estimated
492 before sorting. The enrichment strategy has been demonstrated to be effective in both brightness
493 and lifetime sorting. Combining the enrichment strategy and the multiparameter microfluidic
494 platform allows one to analyze and enrich rare events from a population $>10^8$ within a few hours.
495 Though the enrichment does not provide single cell/analyte resolution, it greatly reduces the time
496 required to search for rare events, thus is an efficient way to analyze or prepare rare events for
497 further investigation or selection with single cell/analyte resolution. It is also feasible to improve
498 the throughput of the multiparameter sorting to ≥ 10 kHz. Together with the new sorting strategy,
499 the speed of droplet-encapsulated rare events analysis and enrichment can potentially exceed
500 FACS, achieving an unprecedented throughput for microfluidics-based cell sorting.

501

502 **Conflicts of interest**

503 There are no conflicts to declare.

504

505 **Acknowledgements**

506 S.M. was supported by the NIH/CU Molecular Biophysics Training Program (T32). This work
507 was supported by the NSF Physics Frontier Center at JILA (PHY 1734006 to R.J.) We
508 acknowledge Nancy Douglas, Connor Thomas, and Annika Ekrem for assistance with cell culture.
509 RJ is a staff member in the Quantum Physics Division of the National Institute of Standards and
510 Technology (NIST). Certain commercial equipment, instruments, or materials are identified in
511 this paper in order to specify the experimental procedure adequately. Such identification is not
512 intended to imply recommendation or endorsement by the NIST, nor is it intended to imply that
513 the materials or equipment identified are necessarily the best available for the purpose.

514

515

516 **References**

- 517 1. N. Inada, N. Fukuda, T. Hayashi, and S. Uchiyama, *Nat. Protoc.*, 2019, **14**, 1293.
- 518
- 519 2. P. H. Lakner, M. G. Monaghan, Y. Möller, M. A. Olayioye, and K. Schenke-Layland, *Sci.*
520 *Rep.*, 2017, **7**, 42730.
- 521
- 522 3. K. Suhling, L. M. Hirvonen, J. A. Levitt, P.-H. Chung, C. Tregidgo, A. Le Marois, D. A.
523 Rusakov, K. Zheng, S. Ameer-Beg, S. Poland, and others, *Med. Photon.*, 2015, **27**, 3–40.
- 524
- 525 4. C. A. Bücherl, A. Bader, A. H. Westphal, S. P. Laptinok, and J. W. Borst, *Protoplasma*,
526 2014, **251**, 383–394.
- 527
- 528 5. M. Benvcina, *Sensors*, 2013, **13**, 16736–16758.
- 529
- 530 6. F.-J. Schmitt, B. Thaa, C. Junghans, M. Vitali, M. Veit, and T. Friedrich, *Biochim. Biophys.*
531 *Acta.*, 2014, **1837**, 1581–1593.
- 532
- 533 7. H.-J. Van Manen, P. Verkuijlen, P. Wittendorp, V. Subramaniam, T. K. Van den Berg, D.
534 Roos, and C. Otto, *Biophys. J.*, 2008, **94**, L67–L69.
- 535

- 536 8. A. Pliss, X. Peng, L. Liu, A. Kuzmin, Y. Wang, J. Qu, Y. Li, and P. N. Prasad, *Theranostics*,
537 2015, **5**, 919–930.
538
- 539 9. A. Margineanu, J. J. Chan, D. J. Kelly, S. C. Warren, D. Flatters, S. Kumar, M. Katan, C. W.
540 Dunsby, and P. M. French, *Sci. Rep.*, 2016, **6**, 28186.
541
- 542 10. R. T. Rebbeck, M. M. Essawy, F. R. Nitu, B. D. Grant, G. D. Gillispie, D. D. Thomas, D. M.
543 Bers, and R. L. Cornea, *SLAS Discov.*, 2017, **22**, 176–186.
544
- 545 11. Y. Long, Y. Stahl, S. Weidtkamp-Peters, M. Postma, W. Zhou, J. Goedhart, M.-I. Sánchez-
546 Pérez, T. W. Gadella, R. Simon, B. Scheres, and others, *Nature*, 2017, **548**, 97–102.
547
- 548 12. C. B. Talbot, J. McGinty, D. M. Grant, E. J. McGhee, D. M. Owen, W. Zhang, T. D.
549 Bunney, I. Munro, B. Isherwood, R. Eagle, and others, *J. Biophotonics*, 2008, **1**, 514–521.
550
- 551 13. S. Kawanabe, Y. Araki, T. Uchimura, and T. Imasaka, *Methods. Appl. Fluoresc.*, 2015, **3**,
552 025006.
553
- 554 14. J. Humpolívcková, J. Weber, J. Starková, E. Masínová, J. Günterová, I. Flaisigová, J.
555 Konvalinka, and T. Majerová, *Sci. Rep.*, 2018, **8**, 10438.
556
- 557 15. X. Dai, Z. Yue, M. E. Eccleston, J. Swartling, N. K. Slater, and C. F. Kaminski,
558 *Nanomedicine*, 2008, **4**, 49–56.
559
- 560 16. G.-J. Bakker, V. Andresen, R. M. Hoffman, and P. Friedl, in *Methods in enzymology*,
561 Elsevier, 2012, vol. 504, pp. 109–125.
562
- 563 17. J. R. Conway, N. O. Carragher, and P. Timpson, *Nat. Rev. Cancer*, 2014, **14**, 314–328.
564
- 565 18. Y. Ardeshirpour, V. Chernomordik, M. Hassan, R. Zielinski, J. Capala, and A.
566 Gandjbakhche, *Clin. Cancer Res.*, 2014, **20**, 3531–3539.
567
- 568 19. P. Manna, S.-T. Hung, S. Mukherjee, P. Friis, D. M. Simpson, M. N. Lo, A. E. Palmer, and
569 R. Jimenez, *Integr. Biol.*, 2018, **10**, 516–526.
570
- 571 20. A. V. Gohar, R. Cao, P. Jenkins, W. Li, J. P. Houston, and K. D. Houston, *Biomed. Opt.*
572 *Express*, 2013, **4**, 1390–1400.
573
- 574 21. J. Sambrano, A. Chigaev, K. S. Nichani, Y. Smagley, L. A. Sklar, and J. P. Houston, *J.*
575 *Biomed. Opt.*, 2018, **23**, 075004.
576
- 577 22. M. Suzuki, I. Sakata, T. Sakai, H. Tomioka, K. Nishigaki, M. Tramier, and M. Coppey-
578 Moisan, *Anal. Biochem.*, 2015, **491**, 10–17.
579
- 580 23. F. Alturkistany, K. Nichani, K. D. Houston, and J. P. Houston, *Cytom. A*, 2019, **95**, 70–79.
581

- 582 24. W. Li, K. D. Houston, and J. P. Houston, *Sci. Rep.*, 2017, **7**, 40341.
583
- 584 25. B. Sands, P. Jenkins, W. J. Peria, M. Naivar, J. P. Houston, and R. Brent, *PloS ONE*, 2014,
585 **9**, e109940.
586
- 587 26. A. I. Skilitsi, T. Turko, D. Cianfarani, S. Barre, W. Uhring, U. Hassiepen, and J. Léonard,
588 *Methods. Appl. Fluoresc.*, 2017, **5**, 034002.
589
- 590 27. J.-C. Baret, O. J. Miller, V. Taly, M. Ryckelynck, A. El-Harrak, L. Frenz, C. Rick, M. L.
591 Samuels, J. B. Hutchison, J. J. Agresti, and others, *Lab Chip*, 2009, **9**, 1850–1858.
592
- 593 28. A. Fallah-Araghi, J.-C. Baret, M. Ryckelynck, and A. D. Griffiths, *Lab Chip*, 2012, **12**, 882–
594 891.
595
- 596 29. L. Mazutis, J. Gilbert, W. L. Ung, D. A. Weitz, A. D. Griffiths, and J. A. Heyman, *Nat.*
597 *Protoc.*, 2013, **8**, 870–891.
598
- 599 30. K. Churski, T. S. Kaminski, S. Jakiela, W. Kamysz, W. Baranska-Rybak, D. B. Weibel, and
600 P. Garstecki, *Lab Chip*, 2012, **12**, 1629–1637.
601
- 602 31. X. Liu, R. Painter, K. Enesa, D. Holmes, G. Whyte, C. Garlisi, F. Monsma, M. Rehak, F.
603 Craig, and C. A. Smith, *Lab Chip*, 2016, **16**, 1636–1643.
604
- 605 32. B. Kintsès, C. Hein, M. F. Mohamed, M. Fischlechner, F. Courtois, C. Lainé, and F.
606 Hollfelder, *Chem. Biol.*, 2012, **19**, 1001–1009.
607
- 608 33. Y. Zhao, A. S. Abdelfattah, Y. Zhao, A. Ruangkittisakul, K. Ballanyi, R. E. Campbell, and
609 D. J. Harrison, *Integr. Biol.*, 2014, **6**, 714–725.
610
- 611 34. B. L. Fiedler, S. Van Buskirk, K. P. Carter, Y. Qin, M. C. Carpenter, A. E. Palmer, and R.
612 Jimenez, *Anal. Chem.*, 2016, **89**, 711–719.
613
- 614 35. E. Papalexí and R. Satija, *Nat. Rev. Immunol.*, 2018, **18**, 35–45.
615
- 616 36. V. Chokkalingam, J. Tel, F. Wimmers, X. Liu, S. Semenov, J. Thiele, C. G. Figdor, and W.
617 T. Huck, *Lab chip*, 2013, **13**, 4740–4744.
618
- 619 37. S. Moon, E. Ceyhan, U. A. Gurkan, and U. Demirci, *PloS ONE*, 2011, **6**, e21580.
620
- 621 38. D. J. Collins, A. Neild, A. DeMello, A.-Q. Liu, and Y. Ai, *Lab Chip*, 2015, **15**, 3439–3459.
622
- 623 39. A. Sciambi and A. R. Abate, *Lab Chip*, 2015, **15**, 47–51.
624
- 625 40. S. Hasan, D. Geissler, K. Wink, A. Hagen, J. J. Heiland, and D. Belder, *Lab Chip*, 2019, **19**,
626 403–409.
627

- 628 41. T.-J. Wu, Y.-K. Tzeng, W.-W. Chang, C.-A. Cheng, Y. Kuo, C.-H. Chien, H.-C. Chang, and
629 J. Yu, *Nat. Nanotechnol.*, 2013, **8**, 682.
630
- 631 42. D. Lando, S. Basu, T. J. Stevens, A. Riddell, K. J. Wohlfahrt, Y. Cao, W. Boucher, M. Leeb,
632 L. P. Atkinson, S. F. Lee, and others, *Nat. Protoc.*, 2018, **13**, 1034–1061.
633
- 634 43. E. Braselmann, A. J. Wierzba, J. T. Polaski, M. Chromiński, Z. E. Holmes, S.-T. Hung, D.
635 Batan, J. R. Wheeler, R. Parker, R. Jimenez, and others, *Nat. Chem. Biol.*, 2018, **14**, 964–
636 971.
637
- 638 44. D.-K. Kang, M. M. Ali, K. Zhang, S. S. Huang, E. Peterson, M. A. Digman, E. Gratton, and
639 W. Zhao, *Nat. Comm.*, 2014, **5**, 5427.
640
- 641 45. C.-Y. Ou, T. Vu, J. T. Grunwald, M. Toledano, J. Zimak, M. Toosky, B. Shen, J. A. Zell, E.
642 Gratton, T. J. Abram, and others, *Lab Chip*, 2019, **19**, 993–1005.
643
- 644 46. P. N. Hedde, T. Abram, T. Vu, W. Zhao, and E. Gratton, *Biomed. Opt. Express*, 2019, **10**,
645 1223–1233.
646
- 647 47. R. Turk-MacLeod, A. Henson, M. Rodriguez-Garcia, G. M. Gibson, G. A. Camarasa, D.
648 Caramelli, M. J. Padgett, and L. Cronin, *PNAS*, 2018, **115**, 5681–5685.
649
- 650 48. J. Myung and S. Hong, *Lab Chip*, 2015, **15**, 4500–4511.
651
- 652 49. T. Lieske, W. Uhring, N. Dumas, A. I. Skilitski, J. Léonard, and D. Fey, *J. Signal Process.*
653 *Syst.*, 2019, **91**, 819–831.
654
- 655 50. Y. Shen, Y. Chen, J. Wu, N. C. Shaner, and R. E. Campbell, *PLoS ONE*, 2017, **12**,
656 e0171257.
657
- 658 51. P. Manna and R. Jimenez, *J. Phys. Chem. B*, 2015, **119**, 4944–4954.
659
- 660 52. Y. Nov, *Appl. Environ. Microbiol.*, 2012, **78**, 258–262.
661
- 662 53. K. S. Sarkisyan, D. A. Bolotin, M. V. Meer, D. R. Usmanova, A. S. Mishin, G. V. Sharonov,
663 D. N. Ivankov, N. G. Bozhanova, M. S. Baranov, O. Soylemez, and others, *Nature*, 2016,
664 **533**, 397–401.
665
666